Nature Environment and Pollution Technology
An International Quarterly Scientific Journal

p-ISSN: 0972-6268 e-ISSN: 2395-3454	Vol. 18	No. 3	pp. 777-787	2019

Original Research Paper | Open Access

Simultaneous Removal of Cu(II) and 1-Naphthol in Wastewater by Magnetic Nanoparticle-Graphene Oxide Composites

Jie Luo*, Donglin Zhao*, Linxia Wang**†, Abdullah M. Asiri**** and Khalid A. Alamry******
*College of Yuanpei, Shaoxing University, Shaoxing, Zhejiang 312000, People's Republic of China
**College of Chemistry and Chemical Engineering, Shaoxing University, Shaoxing, Zhejiang 312000, P. R. China
***School of Materials and Chemical Engineering, Anhui University of Architecture, Hefei 230601, P. R. China
****Chemistry Department, Faculty of Science, King Abdulaziz University, Jeddah 21589, Saudi Arabia
†Corresponding author: Linxia Wang

Nat. Env. & Poll. Tech.
Website: www.neptjournal.com

Received: 19-12-2018
Accepted: 27-02-2019

Key Words:
Graphene composites
Cu(II)
1-naphthol
Magnetic separation

ABSTRACT

A graphene-based magnetic composite (Fe_3O_4/GO) was prepared and used for simultaneous removal of Cu(II) and 1-naphthol. The composite was characterized by SEM, TEM, XRD, FT-IR and Raman. Electron microscopy reflected that Fe_3O_4 spheres were dispersed on graphene layers. The pseudo-second-order kinetic and Langmuir isotherm models could best describe the sorption kinetics and isotherms. The sorption of Cu(II) and 1-naphthol increased with increasing temperature, and thermodynamic parameters calculated from temperature dependent sorption revealed that sorption of Cu(II) and 1-naphthol on Fe_3O_4/GO was spontaneous and endothermic. The results indicated that Fe_3O_4/GO can be utilized as potential adsorbents for purification of co-contaminated water systems.

INTRODUCTION

Discharge of heavy metal ions and organic contaminants into natural waters from different activities such as industries, agriculture and mining is a crucial environmental issue associated negatively with the health and economy. Copper (Cu) is an essential and toxic heavy metal present in wastewater and polluted soils. The ionizable aromatic compounds (e.g., naphthol and naphthylamine) are widely present in the wastewaters discharged from dyestuffs, pesticides, petrochemicals, pharmaceuticals, etc. (Laszlo et al. 2007). The high toxicity and harmful effects of these contaminants seriously jeopardize the health of human and animals by causing diseases such as kidney and liver dysfunction, diarrhoea, damage of bone marrow and loss of calcium from bones. Therefore, it is very significant to develop an effective and suitable method to remove Cu(II) and 1-naphthol from water.

Traditional methods, such as membrane filtration, chemical precipitation, ion exchange, solvent extraction, microbial removal and sorption (Aggarwal et al. 1999, Babel et al. 2003, Bailey et al. 1999, Dabrowski et al. 2004, Hawari et al. 2006, Kuhu 1972, Prasadaao et al. 2006), have been widely used in the removal of organic and inorganic pollutants from aqueous solutions. Among the current techniques for environmental remediation, sorption approach has been applied in large scale for practical application due to a series of advantages such as simple device, easy operation, high security, cost-effective and no secondary pollution (Brown et al. 2000, Sheng et al. 2012, Singh & Tiwari 1997, Zhao et al. 2014). Thus, a series of adsorbent materials such as bentonite, fly ash, activated bamboo charcoal, carbon nanotubes and so on have been tested for the simultaneous removal of inorganic and organic pollutants (Devulapalli et al. 1999, Diaz-Flores et al. 2009, Ma et al. 2010, Wang et al. 2010).

Graphene, a fascinating two dimensional carbon-based material possessing atomic thickness, has attracted the tremendous attentions of researchers. Due to its layered structure, graphene has large theoretical specific surface area (~2600 m^2/g), which makes graphene as a potential adsorbent for environmental pollutant removal (Balandin et al. 2008, Bashmova et al. 2009, Ghosh et al. 2008, Jabeen et al. 2011, Novoselov et al. 2004, Ramesha et al. 2011, Si et al. 2008, Stankovich et al. 2007, Yang et al. 2011, Zhang et al. 2011).

Although graphene has high adsorption ability, it is difficult to be separated from solution phase using traditional separation methods after the adsorption process because of its extremely small particle size and high dispersibility in aqueous solution. Compared with centrifugation and

filtration methods, the magnetic separation method has been considered as a rapid and effective technique for magnetic particles from aqueous solutions. The magnetic recycle performance of materials can effectively avoid the release of nanoscale adsorbent into the natural water, which may give rise to unknown damage to environment. Many magnetic adsorbents based on graphene have been extensively used to remove dyes and metal ions from aqueous solutions (Ai et al. 2011, Chandra et al. 2010, Wang et al. 2011). Magnetite (Fe_3O_4) have drawn considerable attention because of the important scientific interest and the promising applications in magnetic fluids, spintronics, biomedicine, sensors, catalysis, magnetic recording devices, and environmental remediation (Caruso et al. 2001, Liang et al. 2010, Pileni 2001). Fe_3O_4/GO, which has combined properties of graphene and magnetite (Fe_3O_4), possesses some unusual properties such as large surface to volume ratio, low cost, high conductivity and eco-friendliness, will be one of the most excellent methods to reduce organic and inorganic pollutants (He et al. 2010, Li et al. 2012, Li et al. 2011).

The objectives of this study were: (1) to prepare and characterize Fe_3O_4/GO and apply it to remove Cu(II) ions and 1-naphthol from aqueous solution in a batch system; (2) to investigate the mutual effect of Cu(II) ions and 1-naphthol and the sorption mechanism with kinetic, isotherm and thermodynamic models.

MATERIALS AND METHODS

Materials and chemicals: Graphite powder (99.95% purity, average diameter of 25 mm, Qingdao Graphite Co. Ltd., China), 1-naphthol, ammonia solution, $KMnO_4$, sodium acetate (NaAc), H_2SO_4 (98%), H_2O_2 (30%), $FeCl_3 \cdot 6H_2O$, glycol and all other chemicals in analytical purity were purchased from Sinopharm Chemical Reagent Co. Ltd., and used without further purification. Milli-Q (Millipore, Billerica, MA, USA) water was used in all the experiments. The 1-naphthol powders were dissolved in 0.01 $mol.L^{-1}$ NaCl and 100 $mg.L^{-1}$ NaN_3 support electrolyte solution (pH ~ 6.5). The final concentrations of 1-naphthol were limited to <50% of its water solubility to ensure complete dissolution.

Preparation of GO and GO/Fe_3O_4 composites: The sample of GO was fabricated by a modified Hummers method from graphite powder (Hummers et al. 1958). Then the Fe_3O_4/GO was synthesized by solvothermal method. In detail, the as-prepared GO (0.3 g) was dispersed by ultrasonication in 50 mL of ethylene glycol (EG) for more than 2 h. Then 1.0 g of $FeCl_3 \cdot 6H_2O$ and 1.9 g of NaAc were dissolved into the above mixture at ambient temperature. After stirring for ~ 40 min, the solution was transferred into a 100 mL Teflon-lined stainless-steel autoclave and reacted at 190°C for 5 h. The black coloured solution was centrifuged, washed with ethanol several times, and then dried in vacuum oven at 60°C for 24 h.

Characterization: The morphologies of GO and Fe_3O_4/GO were characterized by SEM (JEOL JSM-6700, Tokyo, Japan) and TEM (JEOL-2010, Tokyo, Japan). XRD patterns were measured on a X'Pert PRO diffractometer with Cu K_α radiation (λ=0.154nm). FTIR technique was used in the analysis of the chemical surface groups. FTIR analysis was performed using a Nexus670 FTIR spectrometer (Thermo Nicolet, Madison) equipped with a KBr beam splitter (KBr, FTIR grade). The structural information of GO and GO/Fe_3O_4 were evaluated by a Raman Spectrometer (Model Nanofinder 30R., Tokyo Instruments Inc., Tokyo, Japan). The zeta potential was measured at various pH with a Zetasizer Nano ZS instrument (Malvern Instrument Co., UK) at 25 °C as a function of pH.

Uptake experiments: All the experiments were carried out by using batch techniques in polyethylene centrifuge tubes under ambient conditions. Stock suspension of Fe_3O_4/GO and Cu(II) or 1-naphthol were added in the glass vials to achieve the desired concentrations of different components. The pH was adjusted by adding negligible volumes of 0.01 or 0.1 mol/L NaOH or HNO_3. After the mixture was oscillated for 2 days, the solid and liquid were separated by magnetic separation method. Cu(II) concentration was determined with atomic absorption spectroscopy (AAS). The concentrations of 1-naphthol in the supernatant was determined using a UV-2550 spectrophotometer at wavelength of 332 nm. The removal percentage and sorption capacity of Cu(II) and 1-naphthol were calculated from the difference between the initial concentration (C_0, mg/L) and the equilibrium one (C_e, mg/L). The sorption percentage (adsorption% = $(C_0-C_e)/C_0 \times 100\%$) was derived from the difference of the initial concentration (C_0) and the final one (C_e) in supernatant after centrifugation. All the experimental data were the average of triplicate determination and the relative errors were about 5%.

RESULTS AND DISCUSSION

GO and GO/Fe_3O_4 Composite Characterization

The surface morphology and structure of GO and Fe_3O_4/GO were characterized by SEM and TEM. Figs. 1a and 1c show that GO sheets present lamellar fold structure. Figs. 1b and 1d show that Fe_3O_4/GO particles are not simply mixed up or blended with GO, rather, they are embedded on GO sheets. The Fe_3O_4 spheres are decorated and firmly anchored on the wrinkled graphene layers with a high density. The pleats structure of the graphene may favour to prevent the Fe_3O_4

spheres from agglomeration, while the Fe_3O_4 spheres serve as a stabilizer separate graphene sheets against the aggregation (Zong et al. 2013). Since the vast majority of adsorption sites reside on the surface, Fe_3O_4/GO nanoparticles with higher surface are expected to offer more active adsorption sites on a mass basis than the bulky particles (Guo et al. 2014).

Figs. 2a and 2b present the wide-angle XRD patterns of the synthesized GO and GO/Fe_3O_4. The main peaks at 2θ=30.23°, 35.21°, 43.19°, 53.41°, 57.22° and 62.57° represent the corresponding indices (220) (311) (400) (422) (511) and (440), suggesting the existence of Fe_3O_4 particles in the as-obtained composite. Furthermore, a very slight diffraction peak which is marked with an oval shape at 2θ=10.3° belongs to (001) crystal of GO. Compared to (001) diffraction peak of GO in Fig. 2b, the diffraction peak intensity of Fe_3O_4/GO at 2θ=10.3 is vanished. The absence of the peak at 2θ= 10.3° for composite, suggests the complete exfoliation and reduction of graphite oxide in the preparation process of Fe_3O_4/GO (Guo et al. 2012, Wu et al. 2010, Yao et al. 2012).

The FT-IR spectra of GO and Fe_3O_4/GO samples are shown in Fig. 3. The peaks of epoxy C-O (1220 cm^{-1}) and aromatic C=C (1578 cm^{-1}) can be seen in the FTIR spectrum of GO/Fe_3O_4. The Fe-O characteristic stretching vibration peak at 585 cm^{-1} was observed in Fig. 3b, which proved that Fe_3O_4 was successfully anchored onto graphene sheet (Chang et al. 2012). The FTIR spectrum of GO is also shown in Fig. 3a to make a comparison about the surface functional groups. Several characteristic peaks of GO can be observed, confirming the successful oxidation of graphite. Concretely, C=O (1718 cm^{-1}), aromatic C=C (1620 cm^{-1}), and alkoxy C-O (1100 cm^{-1}) stretching vibrations were observed. We can not see that the peak at 580 cm^{-1} in the FTIR spectrum of GO, indicating that magnetite has been deposited on GO surface (Zhao et al. 2012).

The Raman spectra of GO and Fe_3O_4/GO in Fig. 4 are composed of two characteristic peaks. The peak 1357 cm^{-1} is the D-band corresponding to the disordered sp^2-hybridized carbon atoms of GO while the peak 1605 cm^{-1} is the G-band corresponding to the structural integrity of sp^2-hybridized carbon atoms of GO. The D band is ascribed to structural defects, while G band is the first-order scattering of the E_{2g} vibrational mode in graphite sheets (Tuinstra & Koenig 1970). The D and G bands were also observed at 1357 and 1590 cm^{-1} in Fe_3O_4/GO composites (Fig. 4b). The D band becomes prominent and the intensity ratio of D to G band (I_D/I_G) increases from 0.77 for GO to 1.26 for Fe_3O_4/

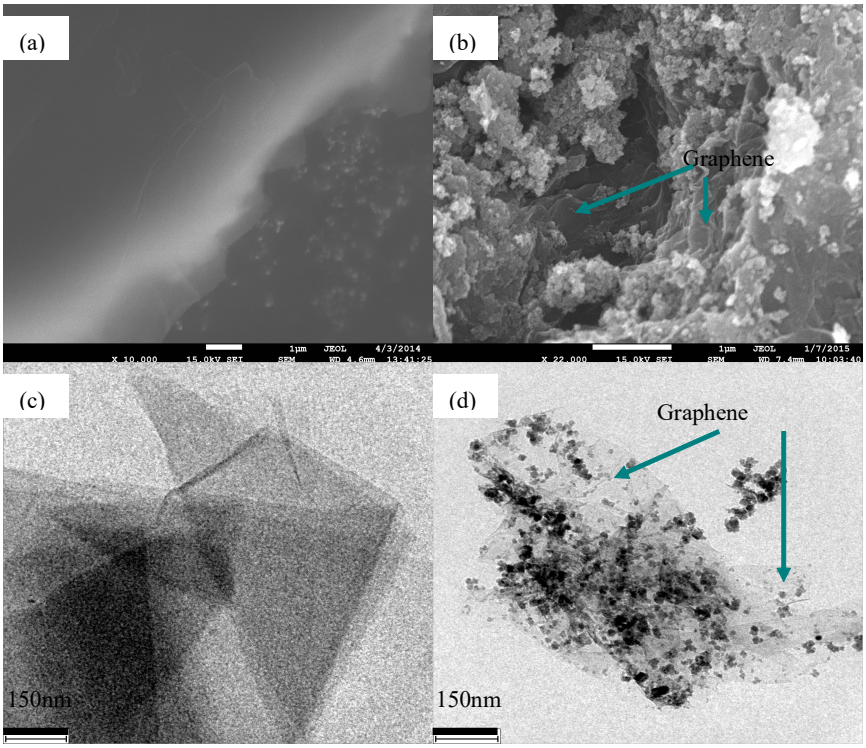

Fig. 1: SEM images of GO (a) and Fe_3O_4/GO (b); TEM images of GO (c) and Fe_3O_4/GO (d).

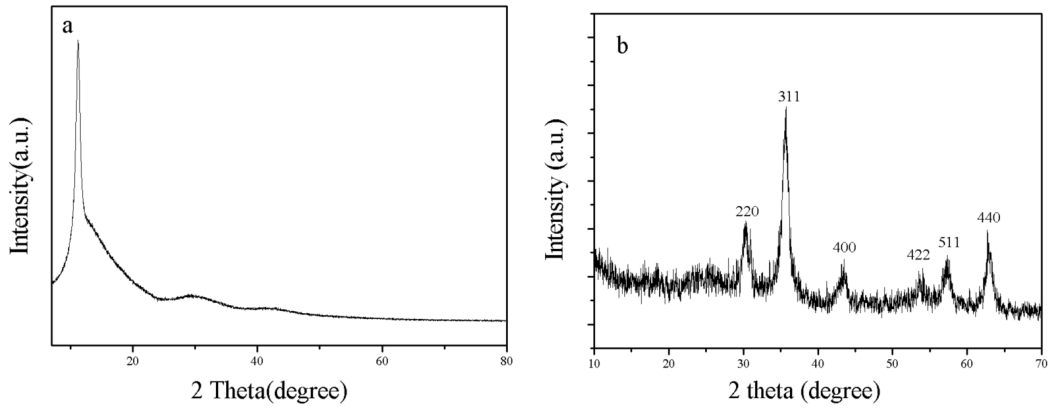

Fig. 2: XRD patterns of GO (a) and Fe_3O_4/GO (b).

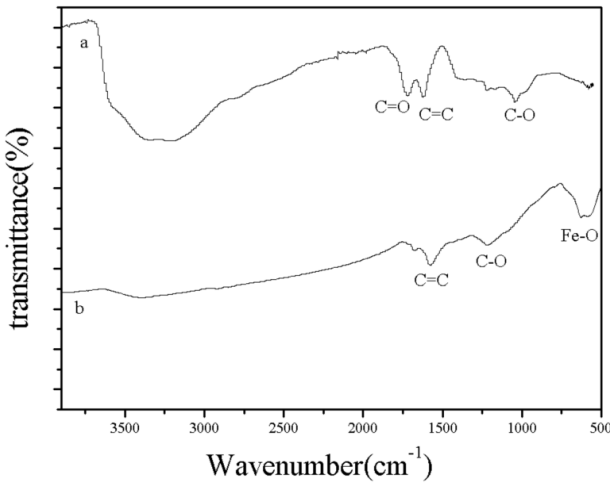

Fig. 3: FITR spectra of GO (a) and Fe_3O_4/GO $_4$ (b).

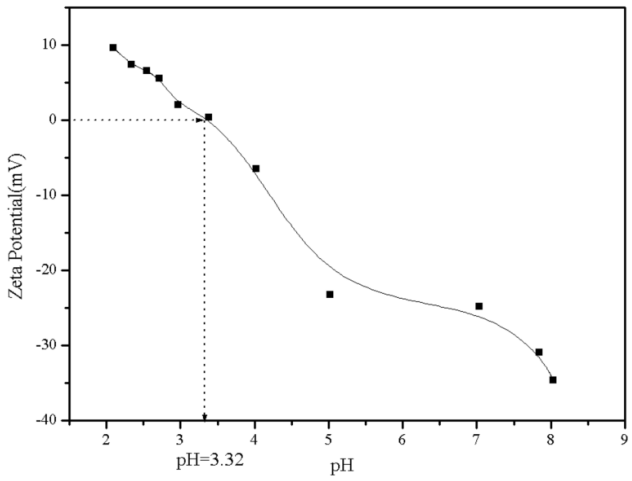

Fig. 5: Zeta potential of Fe_3O_4/GO.

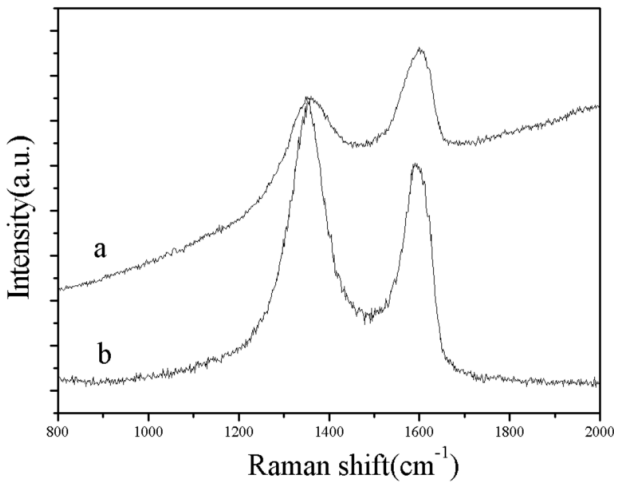

Fig. 4: Raman spectra of GO (a) and Fe_3O_4/GO (b).

GO. This phenomenon has been explained by Stankovich et al. (Stankovich et al. 2007) with the assumption that the reduced state enhances the number of aromatic domains of smaller size in graphene, leading to an increase of the I_D/I_G ratio (Guo et al. 2012).

The pH_{zpc} (point of zero charge) value of Fe_3O_4/GO was calculated to be 3.32 (Fig. 5) from the acid-base titration curve. The surface charge was positive at pH< pH_{zpc}, and was negative at pH> pH_{zpc}.

Single-Solute Sorption Systems

Effect of contact time: As can be seen from Fig. 6a, the sorption of Cu(II) on Fe_3O_4/GO increases with increasing contact time and reach sorption equilibrium within 1 h. Such a short time for reaching sorption equilibrium shows the occurrence of chemical complexation rather than physical

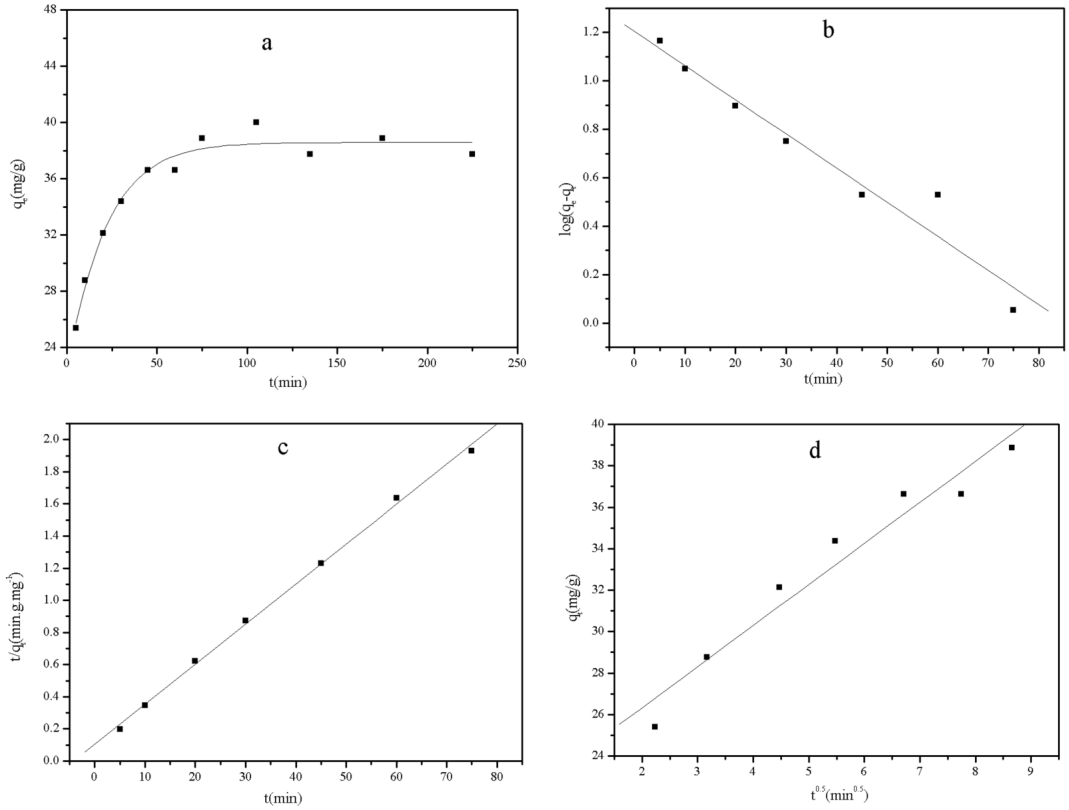

Fig. 6(a): Sorption kinetics of Cu(II) onto Fe_3O_4/GO, symbols represent experimental data, solid lines represent the kinetic model fitting, (b) pseudo-first-order model fitting, (c) pseudo-second-order model fitting, (d) intra-particle diffusion model fitting (pH=6.5±0.1, T=298 *K*, $C_{Cu(II)initial}$=50 mg/L, m/v= 0.4g/L, I=0.01 mol/L NaCl.).

sorption. The fast sorption kinetics is attributed to the rapid migration of Cu(II) from the solution onto the external sites of Fe_3O_4/GO. Fig. 7b shows the sorption kinetics data of 1-naphthol on Fe_3O_4/GO. The sorption of 1-naphthol on Fe_3O_4/GO increases rapidly with increasing contact time and reaches equilibrium after 6.5 h.

The uptake process of Cu(II) and 1-naphthol onto Fe_3O_4/GO can be divided into two stages: (a) an initial fast uptake, and (b) a slow uptake of Cu(II) and 1-naphthol onto Fe_3O_4/GO until an equilibrium was reached. The fast sorption rate in the beginning is attributed to the rapid diffusion of Cu(II) and 1-naphthol from the solution to the external surfaces of Fe_3O_4/GO. In the slow sorption process, Cu(II) ions and 1-naphthol are presumably adsorbed by chelation with the ligands in the interlayer or the ion-exchange in the inner surface of Fe_3O_4/GO. Such slow diffusion will lead to a slow increase in the sorption curve at later stage (Sheng et al. 2014). Moreover, the initial rapid sorption may be owing to an increased number of available sites of Fe_3O_4/GO at the initial stage. The more targets of Cu(II) ions and 1-naphthol can provide higher driving force to facilitate the ions diffusion from the solution to active sites assembly. As time proceeds, the concentration gradients become reduced because of the accumulation of Cu(II) ions and 1-naphthol adsorbed on the surface sites, leading to the decrease in sorption rate at the later stages. According to the sorption kinetics data, a shaking time of 48 h is chosen in the following experiments to ensure complete sorption equilibrium of Cu(II) and 1-naphtholon on Fe_3O_4/GO.

To further study the sorption process, three different kinetic models were used in this study. The pseudo-first-order kinetic model (Sheng et al. 2013) describes the sorption of liquid/solid system based on solid capacity. The pseudo-first-order kinetic equation is expressed as: $q_t = q_e(1-e^{-k_1 t})$, where q_e (mg/g) is the uptake amount at equilibrium time and q_t (mg/g) is the amount adsorbed onto Fe_3O_4/GO at contact time. K_1 is the pseudo-first-order rate constant (h^{-1} or min^{-1}). The pseudo-second order model considers the rate-limiting step as the formation chemisorptive bond involving exchange or sharing of electrons between adsorbate and the adsorbent. The model can be represented by the equation: $t/q_t = 1/(K_2 \cdot q_e^{\,2}) + t/q_e$, where k_2 ($g.mg^{-1}.h^{-1}$) is the

Table 1: The kinetics models for the sorption of Cu(II) and 1-naphtho on Fe_3O_4/GO.

Correlation parameters	Cu(II)	1-naphtho
Pseudo-first-order model		
k_1	0.03(min^{-1})	0.57(h^{-1})
q_e(mg g^{-1})	41.23	108.16
R^2	0.951	0.912
pseudo-second-order model		
k_2	7.29×10^{-3}(g mg^{-1} min^{-1})	7.56×10^{-3}(g mg^{-1} h^{-1})
q_e(mg g^{-1})	39.52	95.63
R^2	0.999	0.969
intra-particle diffusion model		
k_p (mg g^{-1} min^{-1})	1.98(mg g^{-1} min^{-1})	35.12(mg g^{-1} h^{-1})
q_e(mg g^{-1})	42.33	103.77
R^2	0.952	0.971

Table 2: The parameters for Langmuir and Freundlich sorption isotherms of Cu(II).

on Fe_3O_4/GO at different temperatures.						
T(K)	Langmuir			Freundlich		
	q_{max} ($mg\cdot g^{-1}$)	b ($L\cdot mg^{-1}$)	R^2	K_F ($mg^{1-n}\cdot L^n\cdot g^{-1}$)	n	R^2
298	40.78	0.38	0.981	9.69	0.33	0.911
308	61.44	0.42	0.963	11.53	0.46	0.932
318	66.74	0.52	0.981	15.11	0.37	0.906

Table 3: The parameters for Langmuir and Freundlich sorption isotherms of 1-naphthol on Fe_3O_4/GO at different temperatures.

T(K)	Langmuir			Freundlich.		
	q_{max} ($mg\times g^{-1}$)	b ($L\times mg^{-1}$)	R^2	K_F ($mg^{1^n n}\times L^n\times g^{-1}$)	n	R^2
298	98.75	0.11	0.991	24.65	0.249	0.931
308	126.25	0.12	0.989	38.89	0.544	0.943
318	196.31	0.14	0.994	54.29	0.418	0.916

Table 4: Values of thermodynamic parameters for the sorption of Cu(II) on Fe_3O_4/GO.

T(K)	$\Delta G°$ ($kJ\cdot mol^{-1}$)	$\Delta S°$ ($J\cdot mol^{-1}\cdot K^{-1}$)	$\Delta H°$ ($kJ\cdot mol^{-1}$)
298	-19.56	121.5	16.65
308	-20.34	121.5	17.08
318	-21.99	121.5	19.07

Table 5: Values of thermodynamic parameters for the sorption of 1-naphtho on Fe_3O_4/GO.

T(K)	$\Delta G°$ ($kJ\cdot mol^{-1}$)	$\Delta S°$ ($J\cdot mol^{-1}\cdot K^{-1}$)	$\Delta H°$ ($kJ\cdot mol^{-1}$)
298	-24.65	153.1	20.97
308	-25.14	153.1	21.98
318	-26.23	153.1	22.42

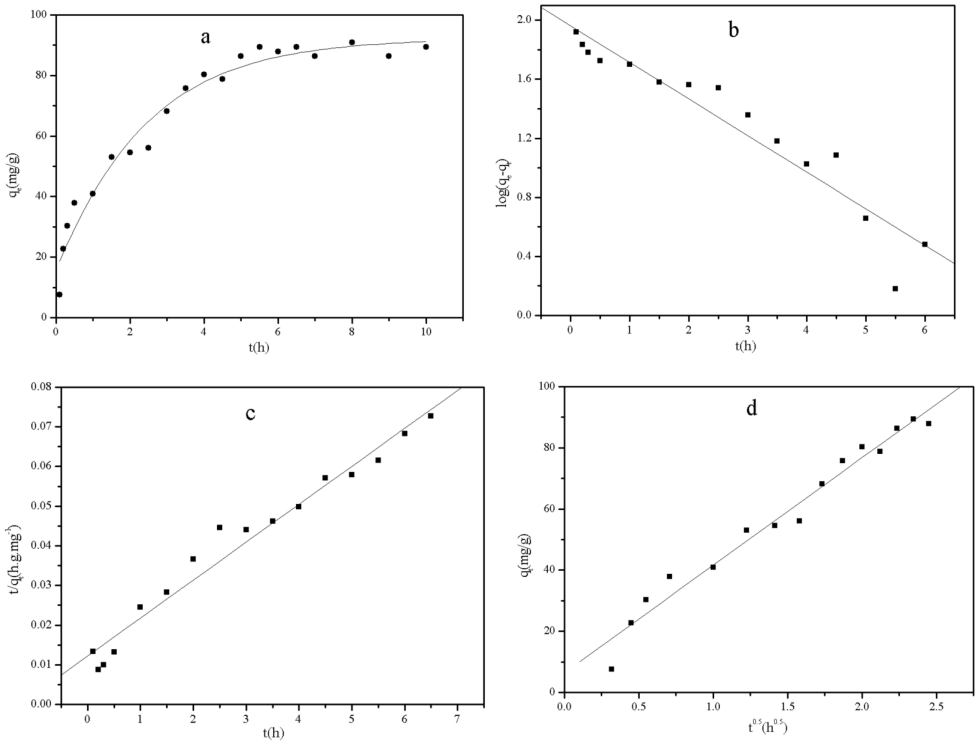

Fig. 7(a): Sorption kinetics of 1-naphthol onto Fe_3O_4/GO, symbols represent experimental data, solid lines represent the kinetic model fitting, (b) pseudo-first-order model fitting, (c) pseudo-second-order model fitting, (d) intra-particle diffusion model fitting (pH=6.5±0.1, T=298 *K*, $C_{1\text{-naphthol initial}}$=50 mg/L, m/v= 0.4g/L, I=0.01 mol/L NaCl).

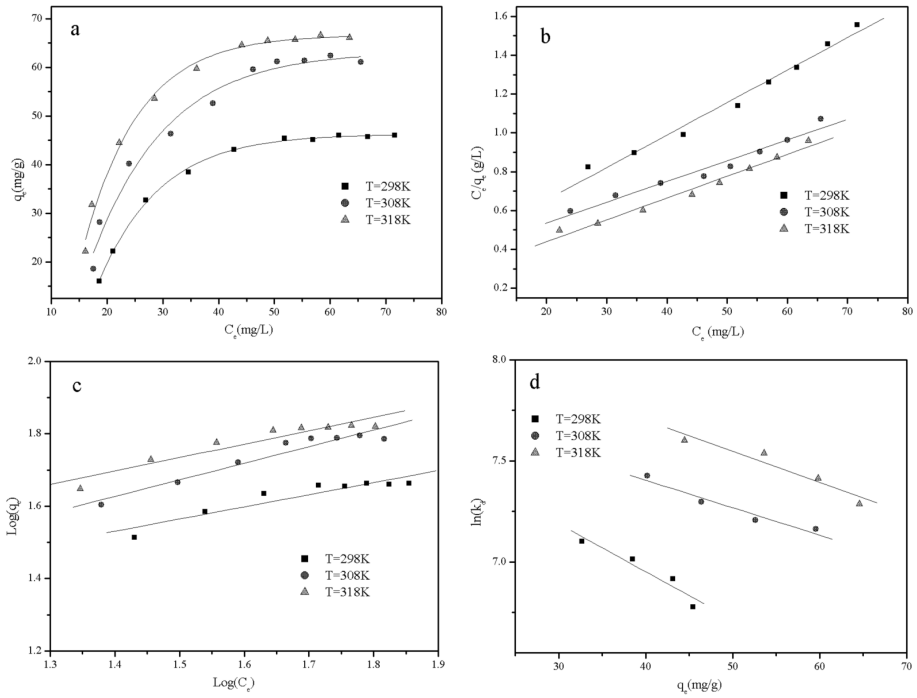

Fig. 8(a): Sorption isotherms, fitting lines of (b) the Langmuir isotherm model and (c) the Freundlich isotherm model of Cu(II) sorption onto Fe_3O_4/GO at different temperatures(pH=6.5±0.1, m/v= 0.4g/L, I=0.01 mol/L NaCl), (d) Linear plots of lnK_d versus q_e.

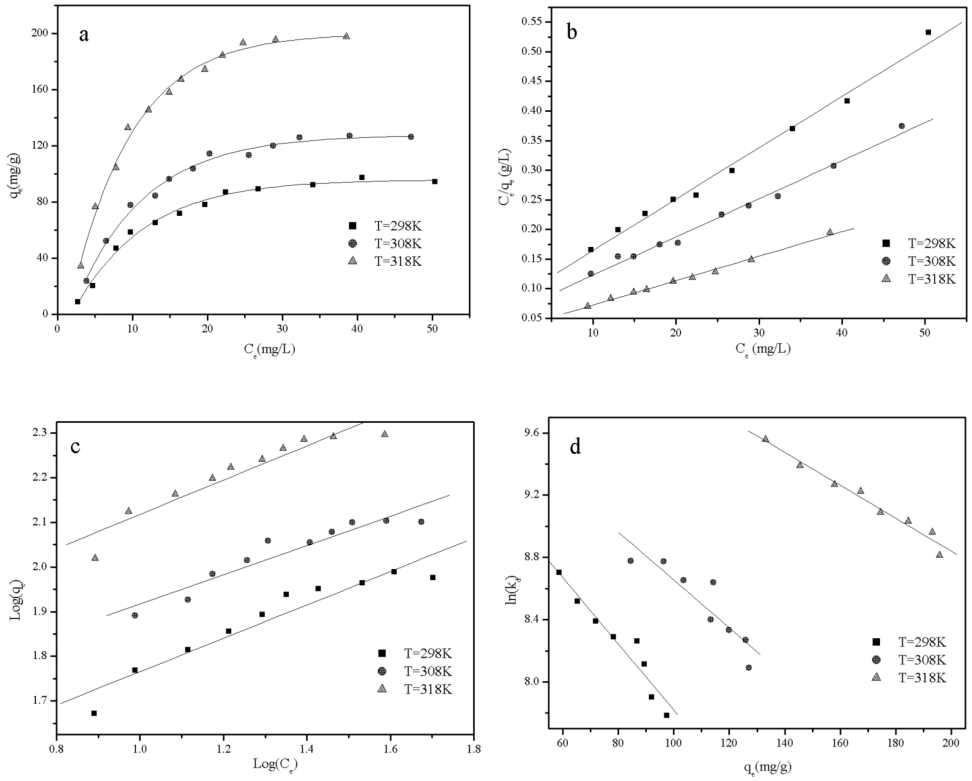

Fig.9(a): Sorption isotherms, fitting lines of (b) the Langmuir isotherm model and (c) the Freundlich isotherm model of 1-naphthol sorption onto Fe_3O_4/GO at different temperatures (pH=6.5±0.1, m/v= 0.4g/L, I=0.01 mol/L NaCl),(d) Linear plots of lnK_d versus q_e.

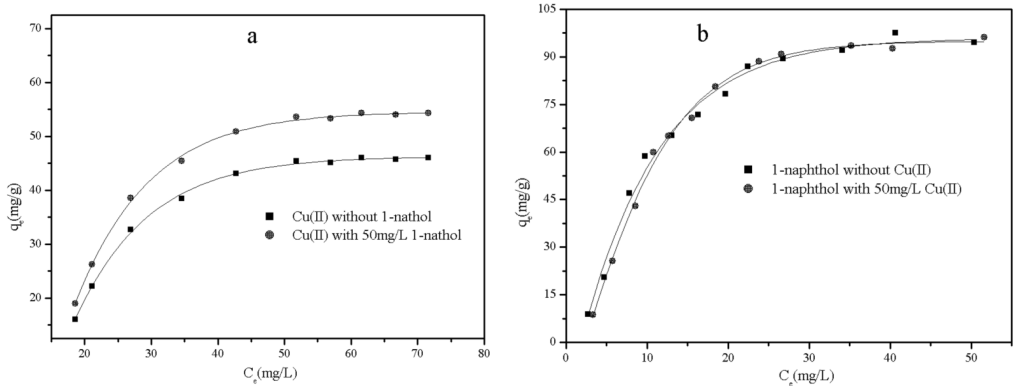

Fig. 10: Sorption isotherms of Cu(II) (a) and 1-naphthol (b) on Fe_3O_4/GO (pH=6.5±0.1, T=298K, m/v= 0.4g/L, I=0.01 mol/L NaCl).

pseudo-second-order rate constant for the sorption, and is a complex function of the initial concentration of solute. The intra-particle diffusion model ($q_t = k_p t^{0.5} + C$, where k_p is the intraparticle diffusion rate constant (mg/(g·$h^{0.5}$), and C is indicative of the intercept of the line (mg/g), which is proportional to the boundary layer thickness) is also used to describe the kinetic uptake of Cu(II) and 1-naphtholon on Fe_3O_4/GO from which the rate-determining step can be ascertained.

Based on the three models (Figs. 6b-d and Figs. 7 b-d), curve fitting was performed and the parameters in the models and regression coefficients (R^2) for the three kinetic models were obtained and given in Table 1. Moreover, the relative coefficient value for the three kinetic models, suggesting that the pseudo-second-order kinetic model fit the sorption of Cu(II) and 1-naphtholon on Fe_3O_4/GO better than the pseudo-first-order and intra-particle diffusion models.

Sorption isotherms and thermodynamic data: Sorption isotherms based on a set of assumptions that are mainly

related to the heterogeneity/homogeneity of sorbents, the type of coverage, and possibility of interaction between the sorbate species, are mathematical models that describe the distribution of the sorbate species among liquid and sorbent. The sorption isotherms for Cu(II) and 1-naphthol onto Fe_3O_4/GO are shown in Fig. 8a and Fig. 9a. Both the sorption amounts of Cu(II) and 1-naphthol increase with increasing equilibrium concentration in solution. Higher concentrations of Cu(II) and 1-naphthol can provide greater driving force for overcoming the mass transfer limitation between the aqueous phase and the bulk phase of Fe_3O_4/GO (Zhang et al. 2014). For both Cu(II) and 1-naphthol, the sorption isotherm is the highest at 318 K and is the lowest at 298 K, suggesting the occurrence of endothermic reaction for Cu(II) and 1-naphthol binding on Fe_3O_4/GO. Changes in the Fe_3O_4/GO pore sizes as well as a rise in the number of sorption sites because of the destroying of some internal bonds near Fe_3O_4/GO surface edge are expected to be achieved at the higher temperature (Genc et al. 2004). Increasing temperature may result in the increase in proportion and activity of Cu(II) and 1-naphthol in solution onto the surface of the sorbent, which may affect the potential of the sorption (Tan et al. 2008). This result shows that the sorption reaction is an endothermic process.

The Langmuir (Fig. 8b and Fig. 9b) and Freundlich isotherm models (Fig. 8c and Fig. 9c) are used to simulate the sorption isotherms and to establish the relationship between the amount of Cu(II) and 1-naphthol adsorbed on Fe_3O_4/GO and the concentration of Cu(II) and 1-naphthol remained in solution. The experimental data are simulated with Langmuir ($q_e = bq_{\max}C_e/(1+bC_e)$) and Freundlich ($q_e = k_F C_e^{\,n}$) models, respectively. In the equations, C_e is residual concentration of adsorbates in solution after sorption equilibration (mol×L^{-1}), q_e is the sorption amount after equilibrium (mol×g^{-1}), $q_{\max}$, the maximum sorption capacity, is the amount of adsorbate at complete monolayer coverage (mol×g^{-1}), b (L×mol^{-1}) is a constant that relates to the heat of sorption, k_F ($mol^{1-n}L^n/g$) represents the sorption capacity and n represents the degree of dependence of sorption at equilibrium concentration. The relative parameters calculated from the three models are listed in Tables 2 and 3.

The Langmuir model assumes that sorption occurs in a monolayer with all sorption sites identical and energetically equivalent. The Freundlich expression is an exponential equation with the assumption of a heterogeneous sorbent surface. This model accommodates several kinds of sorption sites on the solid surface and represents sorption data at low and intermediate concentrations on heterogeneous surfaces. One can see from the R^2 values that Langmuir model simulates the experimental data better than Freundlich model. This result suggests that chemisorption is the principal driving force for Cu(II) and 1-naphthol binding on Fe_3O_4/GO. This phenomenon also shows that chemisorption is the principal removal mechanism in sorption process.

The thermodynamic parameters for Cu(II) and 1-naphthol sorption on Fe_3O_4/GO can be determined from the temperature dependent sorption isotherms, where these parameters, standard entropy change (ΔS^0, J mol^{-1} K^{-1}), the values of standard Gibbs free energy (ΔG^0, kJ mol^{-1}) and standard enthalpy change (ΔH^0, kJ mol^{-1}) of the sorption are useful in defining whether the sorption reaction is exothermic or endothermic, and the spontaneity of the sorption process.

Free energy change ($\Delta G°$) is calculated from the relationship ($\Delta G° = -RT\ln K°$). Where $K°$ is the sorption equilibrium constant. The sorption equilibrium constant, $K°$, can be calculated by plotting lnK_d versus q_e (Fig. 8d and Fig. 9d) and extrapolating q_e to zero. Standard entropy change ($\Delta S°$) is calculated using the equation ($(\partial \Delta G^0/\partial T)_p = -\Delta S^0$). Its intercept with the vertical axis gives the value of lnK°. The average standard enthalpy change ($\Delta H°$) is then calculated from the expression ($\Delta H° = \Delta G° + T\Delta S°$). The relevant data calculated from equations are tabulated in Tables 4 and 5.

The sorption of Cu(II) and 1-naphthol increases with the increasing of temperature and the value of $\Delta H°$ is positive. The positive value of $\Delta H°$ indicates that the sorption of Cu(II) and 1-naphthol on Fe_3O_4/GO is an endothermic process. For Cu(II) and 1-naphthol travel through solution and get to the sorption sites, it is necessary for them to be stripped out of their hydration shell, this process requires energy input. If the exothermicity associated with the sorption of Cu(II) and 1-naphthol on Fe_3O_4/GO does not exceed the dehydration energy of Cu(II) and 1-naphthol, the overall energy balance will result in an endothermic behaviour. The positive value of the standard entropy change (ΔS^0) reflects the affinity of Fe_3O_4/GO toward Cu(II) and 1-naphthol in aqueous solutions and may show some structure changes in the sorbent. The Gibbs free energy change (ΔG^0) is negative and found to be decreasing with rise in temperature, which indicates the feasibility and spontaneity of the sorption process. Ions are readily dehydrated at high temperature and therefore their sorption becomes more favourable. Furthermore, the value of ΔG^0 becomes more negative with increasing temperature, indicating more efficient sorption at higher temperature. The thermodynamic parameters reflect the affinity of Fe_3O_4/GO toward Cu(II) and 1-naphthol in aqueous solutions and may indicate some structural changes in the sorbents.

Binary-Solute Sorption Systems

When 1-naphthol is present in the solution, Cu(II) uptake

on Fe_3O_4/GO is dramatically increased (Fig. 10a). The sequestrated 1-naphthol on Fe_3O_4/GO surfaces becomes a pseudophenolic site (acid active site), which enhances the concentration of acid sites and hence increases the sorption of Cu(II) (Diaz-Flores et al. 2009). The result indicates that 1-naphthol-Cu(II) complex has stronger affinity to Fe_3O_4/GO than Cu(II) ion alone (Wang et al. 2008). But some water-soluble organic chemicals (DOM), often reduce metal ion sorption (Ashworth & Alloway 2007), which is different from 1-naphthol. In general, the sorption of heavy metal ions on material surfaces can be influenced by the coexisting organic components through various interaction mechanisms.

As can be seen from Fig. 10b, the sorption capacity of 1-naphthol on Fe_3O_4/GO is not influenced when Cu(II) is present in solution. Generally, the coexisting metal ions can bridge the organic matters and the solid surface sites, compress the electric double layer, neutralize the negative charges of organic matters and thereby influence the sequestration of organic matters on solid particles.

CONCLUSIONS

In this study, the magnetic graphene oxide composite can be synthesized for the removal of Cu(II) and 1-naphthol from contaminated water. The analysis results of SEM, TEM, XRD, FT-IR and Raman indicate that Fe_3O_4/GO composite is successfully prepared. The Fe_3O_4/GO exhibited favourable removal performance toward Cu(II) and 1-naphthol from the simulated effluent. The kinetics and isotherm experiment data can be well described with the pseudo-second order model and the Langmuir isotherm model, respectively. The thermodynamic parameter (ΔH^0, ΔS^0, and ΔG^0) values of Cu(II) and 1-naphthol sorption onto Fe_3O_4/GO reveal the process is endothermic and spontaneous in nature.

ACKNOWLEDGMENTS

This work was supported by the Public Technology Application Analysis Test Program of Zhejiang(No.2016C37067) and the Project of Shaoxing University (No.2010LG1028).

REFERENCES

Aggarwal, D., Goyal, M. and Bansal, R. 1999. Adsorption of chromium by activated carbon from aqueous solution. Carbon, 37: 1989-1997.

Ai, L.H., Zhang, C.Y. and Chen Z.L. 2011. Removal of methylene blue from aqueous solution by a solvothermal-synthesized graphene/magnetite composite. J. Hazard. Mate., 192: 1515-1524.

Ashworth, D.J. and Alloway, B.J. 2007. Complexation of copper by sewage sludge-derived dissolved organic matter: effects on soil sorption behaviour and plant uptake. Water Air. Soil. Pollut., 182:187-196.

Babel, S. and Kurniawan, T.A. 2003. Low-cost adsorbents for heavy metals uptake from contaminated water: A review. J. Hazard. Mater., 97: 219-243.

Bailey, S.E., Olin, T.J., Bricka, R.M. and Adrian, D.D. 1999. A review of potentially low-cost sorbents for heavy metals. Water Res., 33: 2469-2479.

Balandin, S., Ghosh, W.Z., Bao, I., Calizo, D., Teweldebrhan, F. and Miao, C.N. 2008. Superior thermal conductivity of single-layer graphene. Nano Lett., 8: 902-907.

Bashmova, S. and Bandosz, T.J. 2009. Adsorption/reduction of NO_2 on graphite oxide/iron composites. Ind. Eng. Chem. Res., 48: 10884-10891.

Brown, P., Gill, S. and Allen, S. 2000. Metal removal from wastewater using peat. Water Res., 34: 3907-3916.

Caruso, F., Spasova, M., Susha, A., Giersig, M. and Caruso, R.A. 2001. Magnetic nanocomposite particles and hollow spheres constructed by a sequential layering approach. Chem. Mater., 13: 109-116.

Chandra, V., Park, J., Chun, Y., Lee, J.W., Hwang, I.C. and Kim, K.S. 2010. Water-dispersible magnetite-reduced graphene oxide composites for arsenic removal. ACS Nano., 4: 3979-3986.

Chang, Y.P., Ren, C.L., Qu, J.C. and Chen, X.G. 2012. Preparation and characterization of Fe_3O_4/graphene nanocomposite and investigation of its adsorption performance for aniline and p-chloroaniline. Appl. Surf. Sci., 261: 504-509.

Dabrowski, A., Hubicki, Z., Podko´scielny, P. and Robens, E. 2004. Selective removal of the heavy metal ions from waters and industrial wastewaters by ion-exchange method. Chemosphere, 56: 91-106.

Devulapalli, R. and Jones, F. 1999. Separation of aniline from aqueous solutions using emulsion liquid membranes. J. Hazard. Mate., 70: 157-170.

Diaz-Flores, P.E., López-Urías, F., Terrones M. and Rangel-Mendez J.R. 2009. Simultaneous adsorption of Cd^{2+} and phenol on modified N-doped carbon nanotubes: Experimental and DFT studies. J. Colloid Interface Sci., 334: 124-131.

Genc, H.F., Tjell, J.C. and McConchie, D. 2004. Adsorption of arsenic from water using activated neutralized red mud. Environ. Sci. Technol., 38: 2428-2434.

Ghosh, S., Calizo, I., Teweldebrhan, D., Pokatilov, E.P., Nika, D.L., Balandin, A.A., Bao, W., Miao, F. and Lau, C.N. 2008. Extremely high thermal conductivity of graphene: prospects for thermal management applications in nanoelectronic circuits. Appl. Phys. Lett., 92: 151911-151913.

Guo, J., Wang, R.Y, Tjiu, W.W., Pan, J.S. and Liu, T.X.2012. Synthesis of Fe nanoparticles@graphene composites for environmental applications. J. Hazard. Mater., 225- 226: 63-73.

Guo, X.Y., Du, B., Wei, Q., Yang, J., Hu, L.H., Yan, L.G. and Xu, W.Y. 2014. Synthesis of amino functionalized magnetic graphenes composite material and its application to remove Cr(VI), Pb(II), Hg(II), Cd(II) and Ni(II) from contaminated water. J. Hazard. Mater., 278: 211-220.

Hawari, A.H. and Mulligan, C.N. 2006. Biosorption of lead (II), cadmium (II), copper (II) and nickel (II) by anaerobic granular biomass. Bioresour. Technol., 97: 692-700.

He, H.K. and Gao, C. 2010. Supraparamagnetic, conductive, and processable multifunctional graphene nanosheets coated with high-density Fe_3O_4 nanoparticles. ACS Appl. Mater. Interfaces., 2: 3201-3210.

Hummers, W.S. and Offeman, R.E. 1958. Preparation of graphitic oxide. J. Am. Chem. Soc., 80: 1339-1341.

Jabeen, H., Chandra, V., Jung, S., Lee, J.W., Kim, K.S. and Bin Kim, S. 2011. Enhanced Cr(VI) removal using iron nanoparticle decorated graphene. Nanoscale., 3: 3583-3585.

Kuhu, A.T.1972. Electrochemistry of Cleaner Environments. Plenum Press, New York.

Laszlo, K., Tombacz, E. and Novak, C. 2007. pH-Dependent adsorp-

tion and desorption of phenol and aniline on basic activated carbon. Colloids Surf. A., 306: 95-101.

Liang, J.J., Xu, Y.F., Sui, D., Zhang, L., Huang, Y., Ma, Y.F., Li, F.F. and Chen, Y.S. 2010. Flexible, magnetic, and electrically conductive graphene/Fe_3O_4 paper and its application for magnetic-controlled switches. J. Phys. Chem. C., 114: 17465-17471.

Li, B.J., Cao, H.Q., Shao, J., Qu, M.Z. and Warner, J.H. 2011. Superparamagnetic Fe_3O_4 nanocrystals@graphene composites for energy storage devices. J. Mater. Chem., 21: 5069-5975.

Li, X.Y., Wang X., Song, S.Y., Liu, D.P. and Zhang, H.J. 2012. Selectively deposited noble metal nanoparticles on Fe_3O_4/graphene composites: stable, recyclable and magnetically separable catalysts. Chem. Eur. J., 18: 7601-7607.

Ma, J.W., Wang,F.Y., Huang, Z.H. and Wang, H. 2010. Simultaneous removal of 2,4-dichlorophenol and Cd from soils by electro kinetic remediation combined with activated bamboo charcoal. J. Hazard. Mater., 176: 715-720.

Novoselov, K.S. Geim, A.K., Morozov, S.V., Jiang, D., Y. Zhang, Dubonos, S.V., Grigorieva, I.V. and Firsov, A.A. 2004. Electric field effect in atomically thin carbon films. Science, 306: 666-669.

Pileni, M.P. 2001. Magnetic fluids: Fabrication magnetic properties, and organization of nanocrystals. Adv. Funct. Mater., 5: 323-336.

Prasadaao, T.R., Metilda P. and Gladis JM. 2006. Preconcentration techniques for uranium(VI) and thorium(IV) prior to analytical determination-an overview. Talanta, 68: 1047-1064.

Ramesha, G.K., Vijaya Kumara, A., Muralidhara, H.B. and Sampath, S. 2011. Graphene and graphene oxide as effective adsorbents toward anionic and cationic dyes. J. Colloid Interface Sci., 361: 270-277.

Sheng, G.D., Dong, H.P., Shen, R.P. and Li, Y.M. 2013. Microscopic insights into the temperature-dependent adsorption of Eu(III) onto titanate nanotubes studied by FTIR, XPS, XAFS and batch technique. Chem. Eng. J., 217: 486-494.

Sheng, G.D., Li, Y., Li, Y.M., Dong, H.P., Li, H., Gao, X. and Huang, Y.Y. 2014. EXAFS study of the interfacial interaction of nickel(II) on titanate nanotubes: Role of contact time, pH and humic substances. Chem. Eng. J., 248: 71-78.

Sheng, G.D., Li, Y.M., Yang, X., Ren, X.M. Yang, S.T., Hu, J. and Wang, X.K. 2012. Efficient removal of arsenate by a versatile magnetic graphene oxide composites. RSC Advances, 2: 12400-12407.

Singh, V.K. and Tiwari, P.N. 1997. Removal and recovery of chromium (VI) from industrial waste water. J. Chem. Technol. Biotechnol., 69: 376-382.

Si, Y. and Samulski, E.T. 2008. Synthesis of water soluble graphene. Nano Lett., 8: 1679-1682.

Stankovich, S., Dikin, D.A., Piner, R.D., Kohlhaas, K.A., Kleinhammes, A., Jia, Y.Y. Wu, Y., Nguyen, S.T. and Ruoff, R.S. 2007. Synthesis of graphene-based nanosheets via chemical reduction of exfoliated graphite oxide. Carbon, 45: 1558-1565.

Tan, X.L., Wang, X.K., Geckeis, H. and Rabung, T. 2008. Sorption of Eu(III) on humic acid or fulvic acid bound to hydrous alumina studied by SEM-EDS, XPS, TRLFS, and batch techniques. Environ. Sci. Technol., 42: 6532-6537.

Tuinstra, F. and Koenig, J.L. 1970. Raman spectrum of graphite. J. Chem. Phys., 53: 1126-1130.

Wang, C., Feng, C., Gao, Y., Ma, X., Wu, Q. and Wang, Z. 2011. Preparation of a grapheme based magnetic nanocomposite for the removal of an organic dye from aqueous solution. Chem. Eng. J., 173: 92-97.

Wang, G.H., Zhou, Y.M., Wang, X.G., Chai, X.J., Huang, L. and Deng, N.S. 2010. Simultaneous removal of phenanthrene and lead from artificially contaminated soils with glycine cyclodextrin. J. Hazard. Mate., 184: 690-695.

Wang, Y.J., Jia, D.A., Sun, R.J., Zhu, H.W. and Zhou, D.M. 2008. Adsorption and cosorption of tetracycline and copper(II) on montmorillonite as affected by solution pH. Environ Sci Technol., 42: 3254-3259.

Wu, Z. S., Ren, W., Wen, L., Gao, L., Zhao, J., Chen, Z., Zhou, G., Li, F. and Cheng, H.M. 2010. Graphene anchored with Co_3O_4 nanoparticles as anode of lithium ion batteries with enhanced reversible capacity and cyclic performance. ACS Nano., 4: 3187-3194.

Yang, S.T., Chen, S., Chang, Y.L., Cao, A.N., Liu, Y.F. and Wang, H.F. 2011. Removal of methylene blue from aqueous solution by graphene oxide. J. Colloid Interface Sci., 359: 24-29.

Yao, Y.J., Miao, S.D., Liu, S.Z., Ma, L.P., Sun, H.Q. and Wang, S.B. 2012. Synthesis, characterization, and adsorption properties of magnetic Fe_3O_4@graphene nanocomposite. Chem. Eng. J., 184: 326-332.

Zhang, W.J., Zhou, C.J., Zhou, W.C., Lei, A.H., Zhang, Q.L., Wan, Q. and Zou, B.S. 2011. Fast considerable adsorption of methylene blue dye onto graphene oxide. Bull. Environ. Contam. Toxicol., 87: 86-90.

Zhang, X.B., Wang, Y. and Yang, S.T. 2014. Simultaneous removal of Co(II) and 1-naphthol by core–shell structured Fe_3O_4@cyclodextrin magnetic nanoparticles. Carbohydr. Polym., 114: 521-529.

Zhao, G.X., Wen, T., Yang, X., Yang, S.B., Liao, J.L., Hu, J., Shao, D.D. and Wang, X.K. 2012. Preconcentration of U(VI) ions on few-layered graphene oxide nanosheets from aqueous solutions. Dalton T., 41: 6182-6188.

Zhao, D.L., Liu, C., Liu, J., Zou, S.J. and Li, M. 2014. Preparation and adsorption behaviors of ethylene diamine tetraacetic acid modified zwitterionic hybrid materials, J. Appl. Polym. Sci., 131: 39801-39811.

Zong, P.F., Wang, S.F., Zhao, Y.L., Wang, H., Pan, H. and He, C.H. 2013. Synthesis and application of magnetic graphene/iron oxides composite for the removal of U(VI) from aqueous solutions. Chem. Eng. J., 220: 45-52.